

Simulation of non-Newtonian oil-water core annular flow through return bends

Fan Jiang, Ke Wang, Martin Skote*, Teck Neng Wong, Fei Duan

School of Mechanical and Aerospace Engineering, Nanyang Technological University

50 Nanyang, Avenue, Singapore 639798, Singapore

*Corresponding author. E-mail: mskote@ntu.edu.sg. Tel: +65-67904271

Abstract: The volume of fluid (VOF) model is used together with the continuum surface force (CSF) model to numerically simulate the non-Newtonian oil-water core annular flow across return bends. A comprehensive study is conducted to generate the profiles of pressure, velocity, volume fraction and wall shear stress for different oil properties, flow directions, and bend geometries. It is revealed that the oil core may adhere to the bend wall under certain operating conditions. Through the analysis of the total pressure gradient and fouling angle, suitable bend geometric parameters are identified for avoiding the risk of fouling.

Keywords: non-Newtonian oil-water flow; core annular; VOF model; continuum surface force model; return bend; hydrodynamics

1 Introduction

Due to depleting light oil in the world's reserves, the increasing energy demand the world experiences is leading to the development of heavy crude oils as a source of energy. However, the transport of heavy oils is challenging because of their non-Newtonian characteristics. The most desirable way to transport non-Newtonian oil is core annular flow. In this flow regime, the oil core is located centrally and water flows as an annular film around it. Owing to its industrial importance, the past few decades have seen a number of experimental, analytical and numerical studies on different aspects of core annular flow. One of the earliest investigations was reported by Clark and Shapiro [1]. Subsequently, experimental [2-8], theoretical [9-14] and numerical [15-18] studies have been performed on highly viscous oil-water flow. The main portions of the works undertaken are Newtonian fluids in the pipe. However, the heavy crude

oil has non-Newtonian characterization [19]. The majority of studies of the non-Newtonian flow in pipes focus on single phase flow and gas non-Newtonian flow. Some experimental investigations [20-25] and theoretical studies [26-28] of a non-Newtonian liquid flow across various piping components have been reported. However, non-Newtonian flow through a return bend has rarely been investigated although widely used in the industry.

A return bend connects two parallel straight pipes and reverses the flow direction of the fluids in the second pipe. Flow through return bends is more complex than flow in a straight pipe. When the two-phase flow enters the curved portion, the heavier density fluid is subjected to a large centrifugal force, which causes the liquid to move away from the center of curvature. A few researchers [29-31] studied the hydrodynamics of air-water upflow through return bends, and the results showed that the action of gravitational and centrifugal forces affected the downstream flow pattern after the bend. Furthermore, the return bends did not impact the downstream flow pattern for curvature ratios over 7.1, and also the formation of annular flow was found to be favored by pipe diameters beyond 0.003m. Kerpel et al. [32] investigated two-phase flow behavior and pressure drop of R134a (Newtonian fluid) in a smooth multi-bend. Padilla et al. [33] performed an experiment to visualize the two-phase flow patterns for HFO-1234yf (Newtonian fluid) and R-134a during downward flow in a vertical 6.7 mm inner diameter glass return bend. Meng et al. [34] conducted a series of experiments to study the two-phase flow of refrigerant R141b (Newtonian fluid) in vertical and declined serpentine tubes of inner diameter 6 mm and used a volume of fluid (VOF) model with phase change to simulate the flow and heat transfer.

Recently, investigations of the liquid-liquid flow through a return bend have been reported. Sharma et al. [35] investigated the hydrodynamics of kerosene-water flow through return bends, and observed that the bend geometry strongly influences the downstream phase distribution. In addition, pressure drop correlations were proposed. Later, Sharma et al. [36] reported the hydrodynamics of highly viscous oil-water flow cross return bends, and noted that the direction of two-phase flow across the bend impacted on the downstream phase distribution. Ghosh et al. [37] used the computational fluid dynamic (CFD)

software FLUENT to analyze the core annular flow of heavy oil-water (Newtonian fluids) through return bends, and reported that the simulation results agreed with the experimental observations. Furthermore, the profiles of velocity, pressure, and volume fraction were studied. Jiang et al. [38] numerical analyzed the non-Newtonian oil and water core annular flow through a Π bend, and discussed the effects of some factors on flow hydrodynamic. However, almost nothing is known about the effect of return bends on the hydrodynamics of liquid non-Newtonian liquid flow. Therefore, it is of value to investigate the flow of water and non-Newtonian oil through the return bends, because in industrial applications the non-Newtonian oil is usually transported through return bends.

In the present work, the VOF and the continuum surface force (CSF) models are used to simulate the core annular flow of water and non-Newtonian oil through return bends. The various flow parameters and the effect of different oil properties and bend geometry on core annular flow are discussed. The results provide suitable operation conditions for designing the U-bend pipefitting. The remainder of the paper is organized as follows. In Section 2, the mathematical model is derived based on Navier-Stokes (N-S) equations and CSF model. In Section 3, the conditions of the numerical simulation are described. In Section 4, the regime of the flow parameters influenced by oil properties and bend geometry are discussed. The conclusions drawn in this paper are presented in Section 5.

2. Mathematical model

2.1 Governing equations

(1) Continuity equation,

$$\frac{\partial \rho}{\partial t} + \nabla \cdot (\rho \vec{v}) = 0 \quad (1)$$

where t is time; ρ is the volume averaged density, $\rho = \alpha_o \rho_o + \alpha_w \rho_w$, α_o is the volume fraction of oil, α_w is the volume fraction of water; ρ_o is the density of oil, ρ_w is the density of water; and \vec{v} is velocity.

(2) Momentum equations,

$$\frac{\partial(\rho\vec{v})}{\partial t} + \nabla \cdot (\rho\vec{v}\vec{v}) = -\nabla p + \nabla \cdot [\mu(\nabla\vec{v} + \nabla\vec{v}^T)] + \rho\vec{g} + \vec{F} \quad (2)$$

where p is pressure; \vec{g} is gravity acceleration; superscript ' T ' indicates transpose; μ is the shear viscosity, $\mu = \alpha_o\mu_o + \alpha_w\mu_w$, μ_o is the viscosity of oil, μ_w is the viscosity of water; and \vec{F} is the external body forces including the gravity, centrifugal and buoyancy forces.

In the case of non-Newtonian oil water flow through the bend, the velocity is very low and the viscosity of the non-Newtonian oil is high ($Re_m = Dv_m\rho_m / \mu_m = 3566.46$, which is less than 4000), hence the core flow is considered as laminar. Since the flow is laminar, the Navier-Stokes equations can be solved directly (without turbulence modelling) although the requirement on resolution is much less restricted compared to direct numerical simulations of turbulent flows (see further references in e.g. [39]).

(3) Boundary conditions

The boundary conditions are defined as:

- a) The uniform velocity distribution is normal to the inlet plane where the oil is present in the center of the inlet plane, while the water forms the outer ring plane. In each of the two regions, the velocity profile is constant and volume fraction is unity for oil and water, respectively. Hence $v = v_o$ for $r \leq D_1$, and $v = v_w$ for $D_1 < r \leq D$, where v is the horizontal velocity component and r is the radial coordinate, see Fig. 1 for definitions of r, D, D_1 .
- b) $p = 0$ is used in the outlet plane.
- c) $\vec{v} = 0$ is used as the wall boundary i.e. no slip or penetration. In addition, the contact angle between water and pipe material is also specified at the wall.

2.2 Surface tension and wall adhesion

The VOF method includes the influence of surface tension along the interface between the two phases. The surface tension is modeled using the continuum surface force (CSF) model [40], whereby the surface tension can be written in the following form:

$$F = \sigma_{pq} \frac{\rho \kappa_q \nabla \alpha_q}{\frac{1}{2}(\rho_p + \rho_q)} \quad (3)$$

where σ_{pq} is surface tension coefficient between the p -th phase and the q -th phase; κ_t is curvature,

$$\kappa_t = \nabla \cdot \frac{\nabla \alpha_t}{|\nabla \alpha_t|}$$

2.3 Power law for non-Newtonian viscosity

In this work, the heavy oil is considered a non-Newtonian fluid, which is modeled according to the following power law for the non-Newtonian viscosity:

$$\mu = K(\dot{\gamma})^{n-1} \quad (4)$$

where K is a consistency index and n is a flow behavior index, both chosen empirically, $\dot{\gamma}$ is the shear rate. If $n < 1$, the non-Newtonian fluid is called shear-thinning fluid, if $n > 1$, it is a shear-thickening fluid, and if $n=1$, it is a Newtonian fluid. In the present study, the shear-thinning non-Newtonian fluid and Newtonian fluid are considered.

3. Numerical solution

The commercial CFD software package ANSYS FLUENT 14.5 has been used for the simulation of non-Newtonian oil and water flow through return bends. The governing equations are discretized using the finite volume method. The equations are subsequently solved using a segregated solver. In the simulation, the following assumptions are made: (1) each phase is an isothermal and incompressible fluid; (2) a single pressure is shared by both phase; (3) continuity and momentum equations are solved for each phase; (4) the two fluids are immiscible; (5) the co-axial entry of liquids is made by straight nozzles; (6) the flow developing downstream is obtained by using a transient numerical procedure assuming an initial condition of core annular flow; (7) a fully developed flow exists when the bend is reached after the inlet length (0.15m).

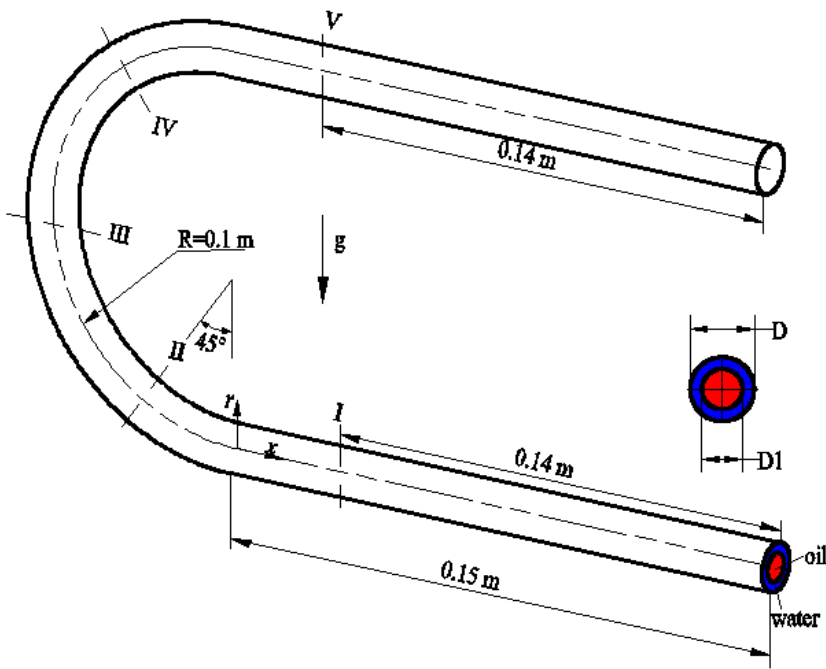


Fig. 1 Schematic of model geometry.

3.1. Geometry

The computational domain consists of a pipe of 0.012 m diameter (D) with a U-type form, and is depicted in Fig. 1. The radius of the center-line curvature (R) of the return bend is 0.1 m (its range is 100-300 mm) and the curvature ratio ($2R/D$) is 16.67. In order to establish the core annular flow, co-axial entry (nozzle) of both fluids with non-Newtonian oil at the center ($D1$), and water at the annulus area ($D-D1$) has been considered as shown in Fig. 1. The variation in $D1$ is in the range of 7-10 mm. For a clear presentation of the flow phenomenon in the return bend, five cross-sections (I-V) at different locations are considered as indicated in the figure. The present geometry is identical to the experimental study in [35-36].

3.2 Meshing of the computational domain

The mesh of computational domain has been generated in the software ANSYS Workbench. Fig. 2 shows the grid of the complete return bend, which consists of 68894 hexahedral cells and 76293 nodes. Examination of the mesh was performed in order to ensure that the skewness is below 0.9 for the

hexahedral meshes. In addition, the dependence of the results on cell number is checked by performing simulations of many cases with different cell numbers, and the results are presented in Fig. 3 which shows the oil phase volume fraction (α_o) calculated as the mean value from position I and V. The result from the various mesh sizes are compared for different volumetric flow rates of oil and water, reflected in the parameter β which will be explained in section 4.1, together with the empirical data included in Fig. 3. These mesh independence investigations reveal that the results are independent of the grids for the current set of cells.

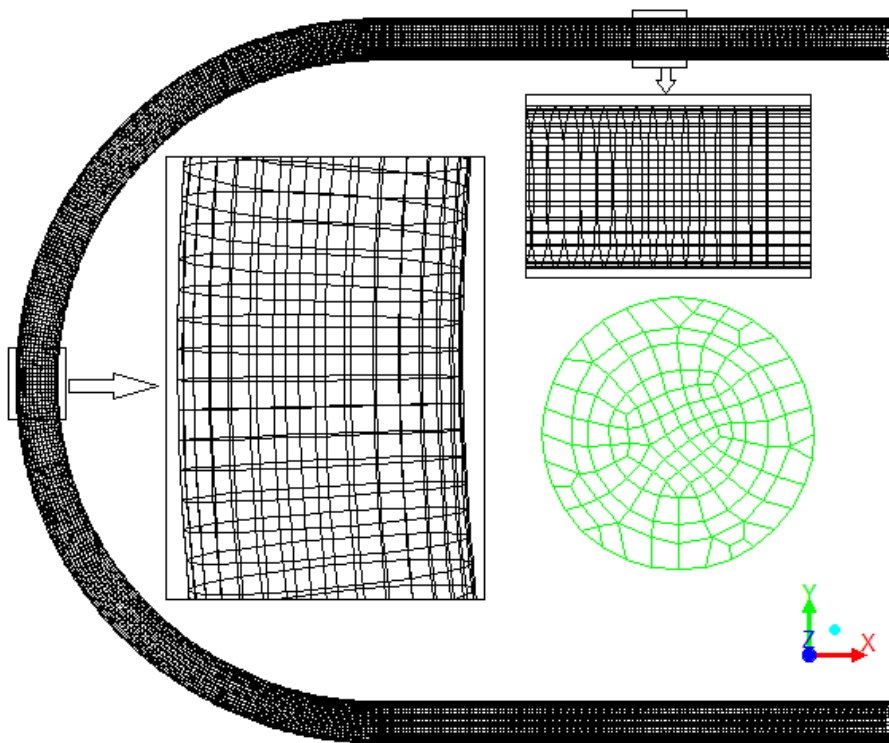


Fig. 2 The computational mesh distribution.

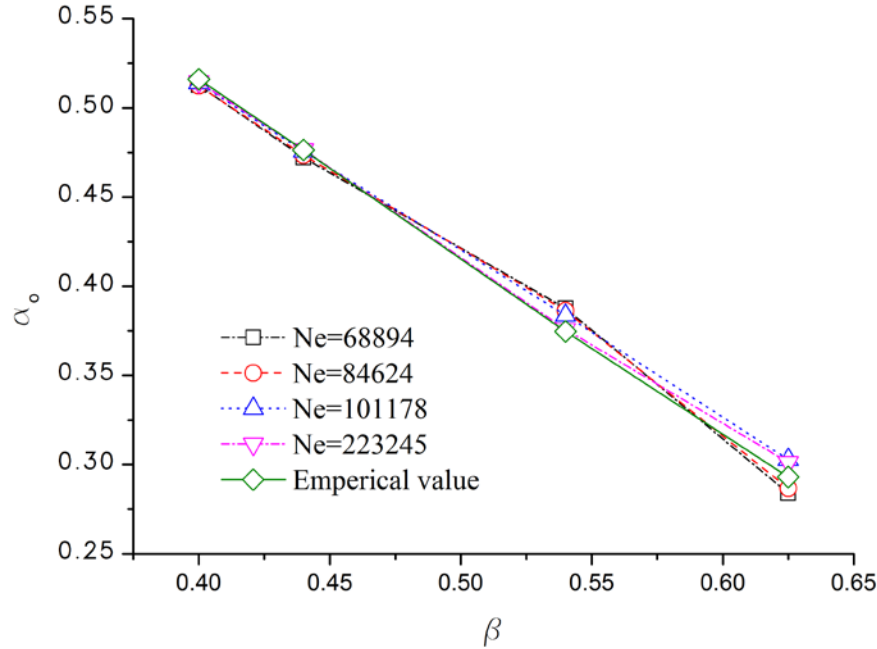


Fig. 3 Effect of element numbers (**Ne**). The empirical values are given according to the expression $\alpha_o = 1 - \beta[1 + 0.35(1 - \beta)]$ and are taken from [36].

3.3 Solution strategy

Different approaches of discretization of the governing equations are used. The continuity equation is discretized by the PRESTO! scheme while the momentum equations are discretized by the first order upwind scheme (due to the stability of this scheme while the precision satisfies engineering requirement). The pressure-velocity coupling is solved by the PISO algorithm [41-42]. In general, these schemes ensured satisfactory accuracy, stability and convergence. In order to observe the core annular flow forming behavior of the two-phase flow and to ensure a Courant number less than unity, a transient simulation with a time step of 0.0001s is performed.

In this study, the numerical computation is considered converged when the residual of each variable is lowered by a factor 0.001 times the initial residual value. A laminar non-Newtonian power law model for the non-Newtonian oil is chosen.

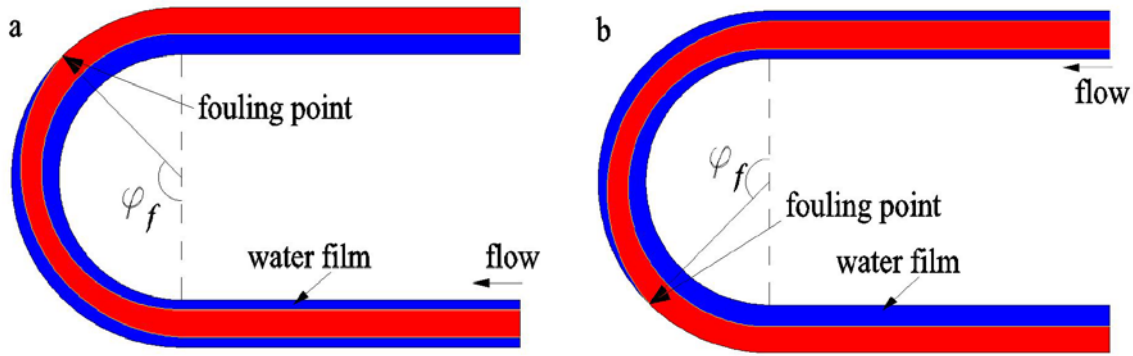


Fig. 4 Definition of fouling angle. a) fouling angle of upflow; b) fouling angle of downflow. ■ oil, ■ water.

3.4 The hydrodynamic parameters

(1) Total pressure gradient, k

$$k = \Delta p / 2R \quad (5)$$

where Δp is the total pressure drop between cross-section I and V (see Fig. 1) in bend pipe; R is the bend radius.

(2) Fouling characteristics, φ_f

Fouling can cause serious problem during transportation of non-Newtonian oils. From the experiments of Sharma et al. [35-36], fouling could happen at the bend under specific operating conditions. The point at which the water film sticks to the pipe wall is considered as the initiation point of fouling (the criterion for oil fouling the wall is that the volume fraction of oil is more than 0.9). Geometrically, this point was defined as the corresponding angle of the bend (fouling angle, φ_f) by Ghosh et al. [37], and is reproduced in Fig. 4 for convenience.

4. Results and discussion

4.1 Validation of the model with experimental results

Since there are no experimental results of non-Newtonian oil and water two-phase flow through return bends, a simulation with Newtonian oil (lube oil, $\rho = 960 \text{ kg/m}^3$, $\mu = 0.2 \text{ Pa}\cdot\text{s}$, $\sigma = 0.039 \text{ N/m}$) was carried out initially under the experimental condition reported by Sharma et al. [36]. Fig. 3 compares the

simulated results and the empirical values, and presents the predicted oil phase volume fraction (α_o), which is calculated as the mean value from positions I and V, for four different values inlet volume fraction of water (β). The empirical values shown in Fig. 3 is given according the formula valid for $\alpha_o = 1 - \beta[1 + 0.35(1 - \beta)]$ where $\beta = Q_w / (Q_w + Q_o)$ with Q_w and Q_o as the volumetric flow rates of water and oil, respectively. The expression, which is valid for straight pipes, was first proposed by Arney et al. [4]. The values from the current simulation are very close to the empirical values [36], which indicate that the VOF model is capable of capturing the physical phenomena of a core annular flow.

4.2 Hydrodynamics analysis of core annular flow

Subsequently, simulations were conducted for non-Newtonian oil properties (properties of non-Newtonian oil are shown in Table 1). The additional information on the hydrodynamics of non-Newtonian oil and water core annular flow, are presented in Figs. 5-8. In this CFD calculation, the annular downflow corresponding to $v_{so}=0.15\text{m/s}$ (oil superficial velocity) and $v_{sw}=0.3\text{m/s}$ (water superficial velocity) is analyzed. In this section, the non-Newtonian oil is CMC1.

Table 1 Physical properties of non-Newtonian oil.

Oil name	Density (kg/m^3)	Fluid consistency coefficient	Flow behavior index	Surface tension (N/m)
CMC1 [43]	999.9	0.089	0.789	0.0714
CMC2 [43]	1000.0	0.469	0.658	0.0718
CMC3 [43]	1000.4	0.972	0.615	0.0727
CMC4 [44]	1000.8	0.00218	0.948	0.0735
CMC5 [44]	1001.2	0.00419	0.910	0.0745
CMC6 [44]	1001.3	0.00588	0.871	0.075
CMC7 [44]	1001.5	0.00692	0.850	0.0755

At first, the total pressure field in the return bend was estimated, and the sectional contour of total pressure and the radial profiles of total pressure at lines of different sections are depicted in Fig. 5. Fig. 5a shows the total pressure contours in longitudinal and transverse sections, and it is clear that the total pressure decreases gradually as the oil-water mixture flows downstream. Furthermore, the cross-section plots indicated that the total pressure in the center is higher than at the wall. Fig. 5b shows the radial

variation of total pressure along the centerline at five different cross-sections (cross-section I-V in Fig. 1), and it is noted that the total pressure distribution does not vary much (the distribution curve is almost a straight line) at the upstream positions III-V, while it is changed to an inclined curve at the downstream positions I-II, illustrating the cross-flow pressure gradient occurring due to the bend.

Fig. 6 represents the velocity contour and radial profiles of velocity at different sections. Fig. 6a depicts the velocity contour of longitudinal and transverse sections. From Fig. 6a it can be deduced that the velocity is higher at the center and gradually decreases to zero at the wall, and increases as the two-phase flow moves towards the outlet. Fig. 6b shows the velocity profiles at five different cross-sections, from which it is clear that the velocity profile is flat at the positions III-V and is changed to a crested curve for the downstream positions.

The core configurations at different sections together with the radial profiles of the oil volume fraction are shown in Fig. 7. Fig. 7a depicts the contour of the oil volume fraction in longitudinal and transverse sections, and it can be concluded that the flow can maintain the core annular state at upstream positions V and IV, while the oil adheres to the wall near section III of the curved portion. The reason is the effects of the centrifugal force, which draws the oil to the wall. Fig. 7b shows the profile of oil volume fraction, and also presents the fouling phenomenon of oil clinging to the pipe wall.

Fig. 8 shows the distribution of wall shear stress at different sections. Note that the maximum value of wall shear stress occurs near section III of the curved portion, because in this location, the non-Newtonian oil adheres to the wall, and tends to increase the wall shear stress. Combining the wall shear stress distribution with the oil fraction shown in Fig. 7, the positions where the oil touches the wall indicate that the oil in the pipe will penetrate through the water annular flow and positions where the oil is touching the wall is where the maximum wall shear stress occurs.

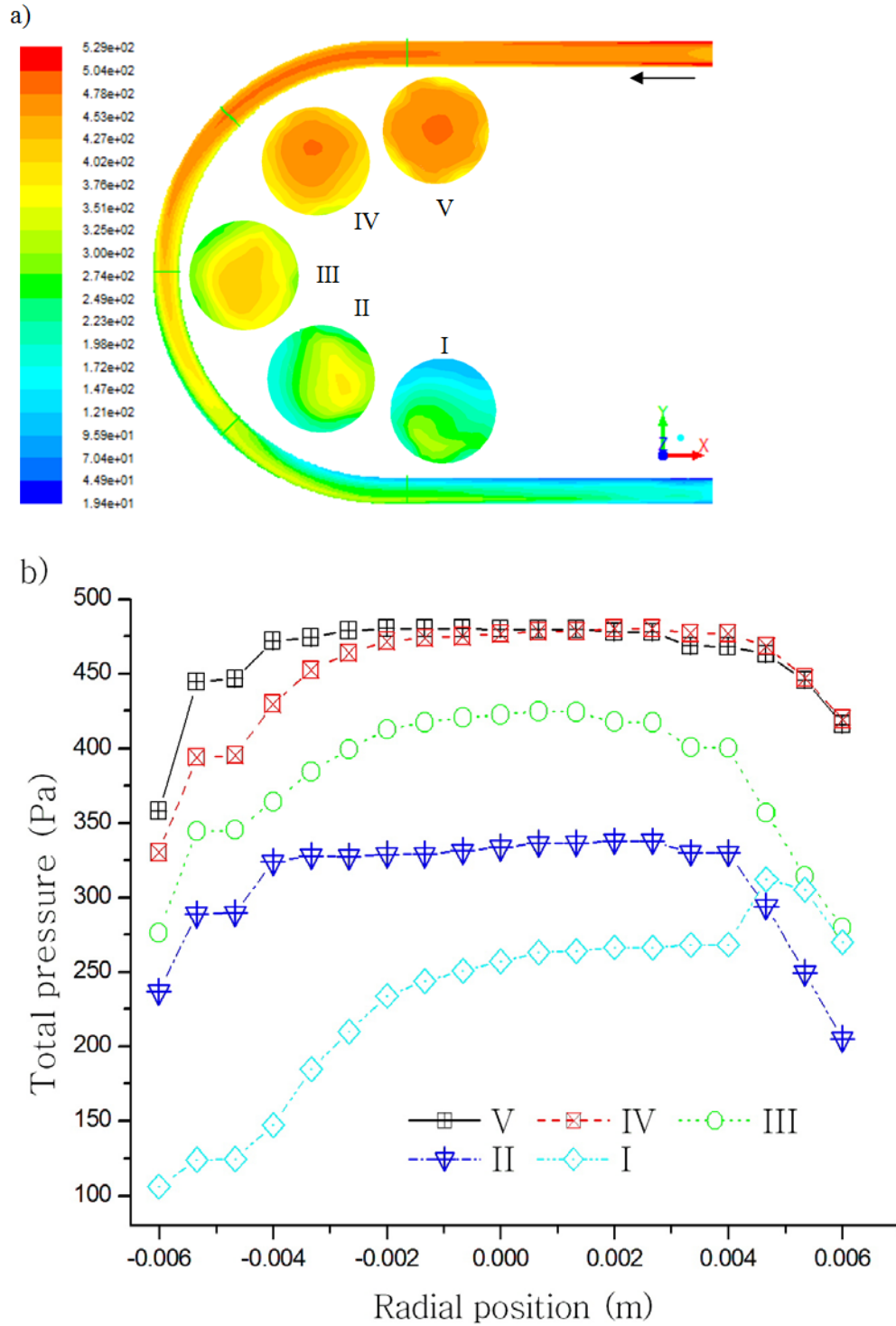


Fig. 5 Contour and radial distribution of total pressure at different cross-sections. a) total pressure contour at different cross-sections; b) radial total pressure profiles at lines of different cross-sections.

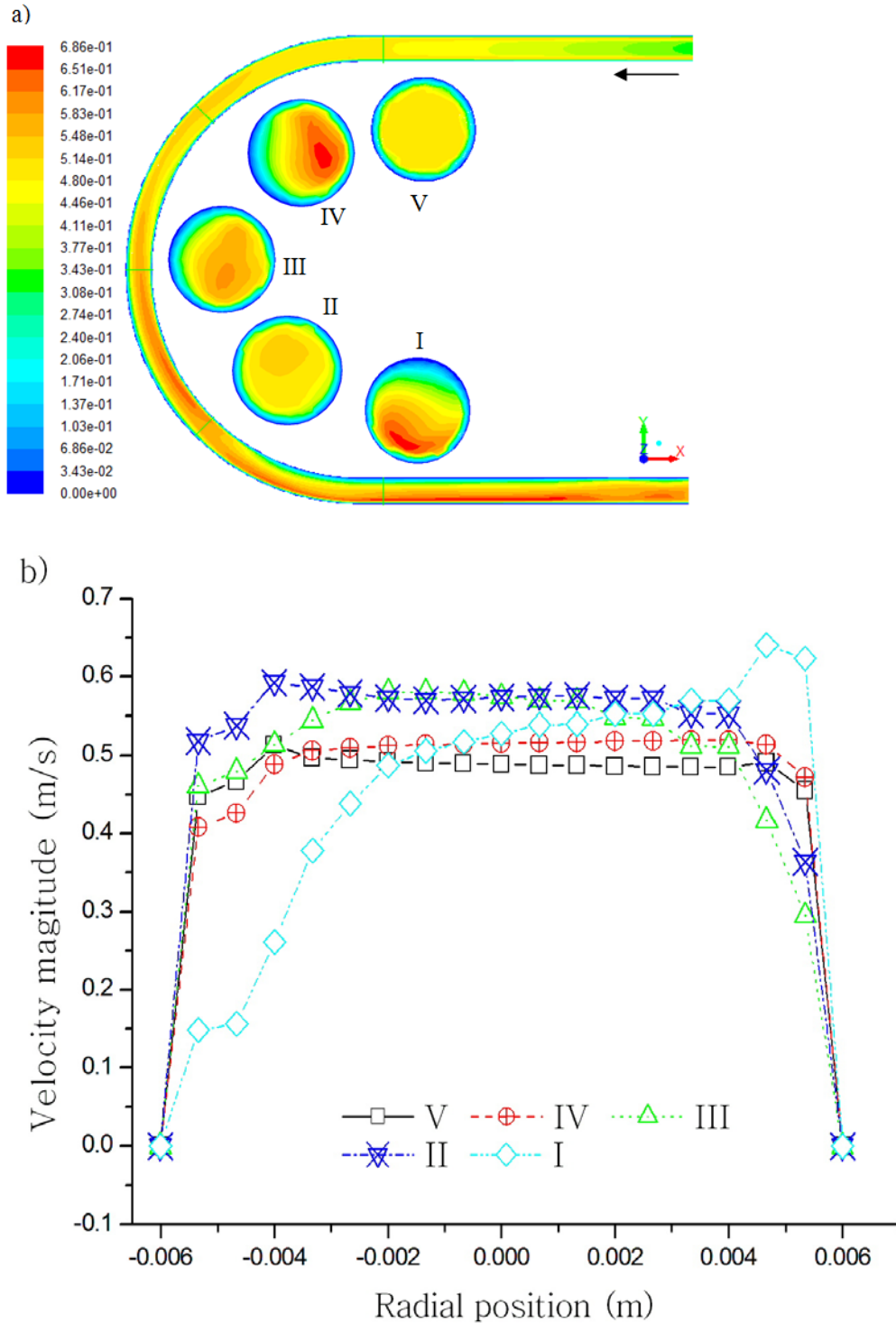


Fig. 6 Contour and radial distribution of velocity at different cross-sections. a) velocity contour at different cross-sections; b) radial velocity profiles at lines of different cross-sections.

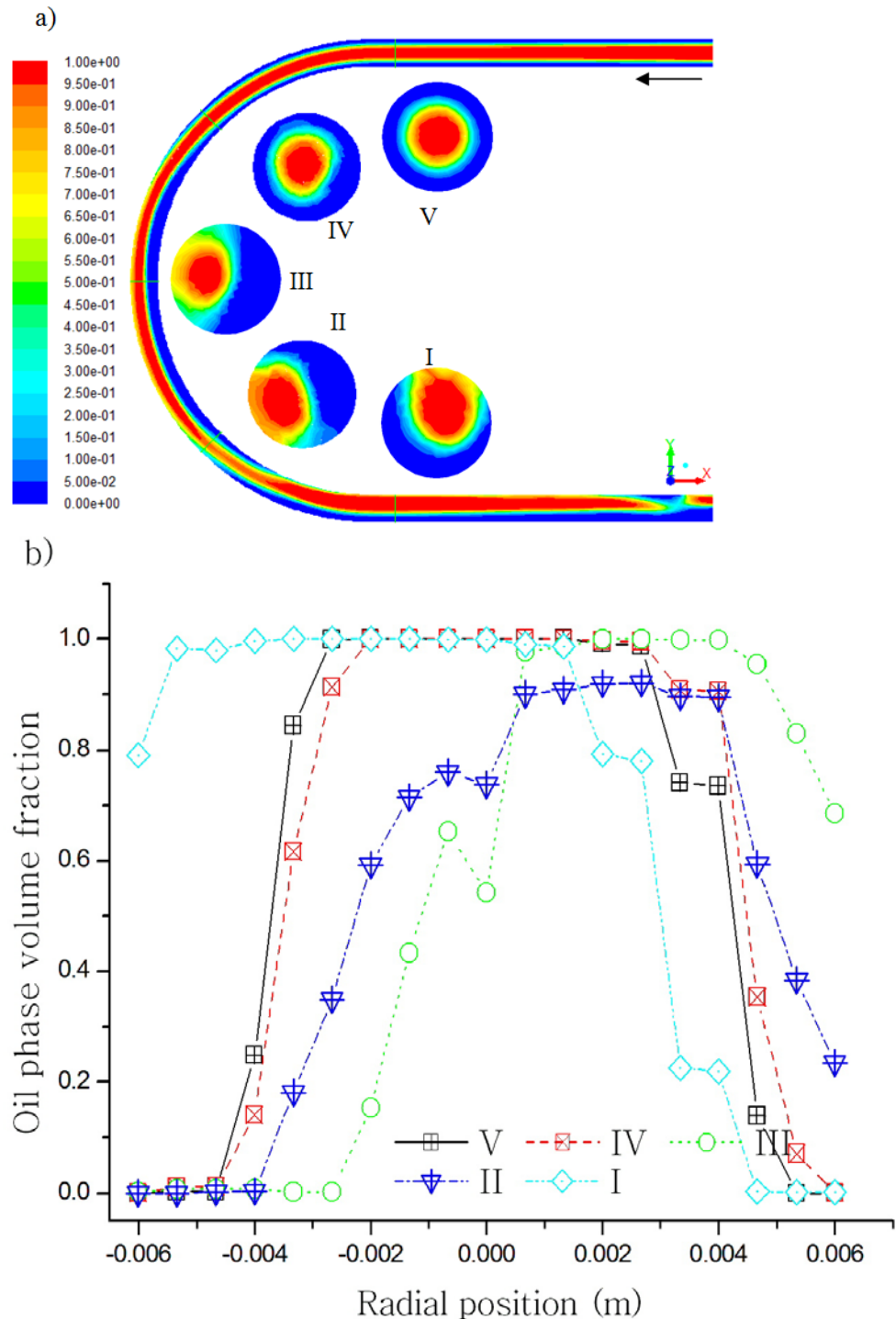


Fig. 7 Contour and radial distribution of oil volume fraction at different cross-sections. a) contour at different cross-sections; b) radial profiles at different cross-sections.

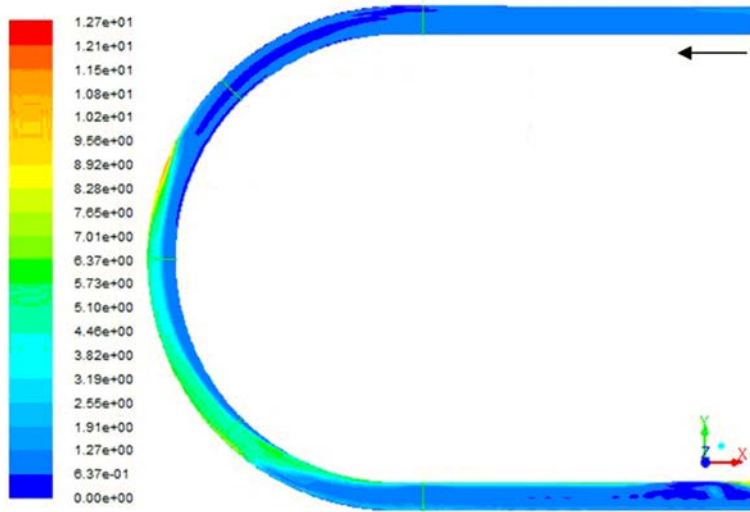


Fig. 8 Contour of wall shear stress.

4.3 The effect of non-Newtonian parameters on the flow field

Further studies have been directed to understand the variation of total pressure gradient (k) and fouling angle (φ_f) with different non-Newtonian oil properties. Fig. 9 depicts the variation of total pressure gradient (k) and fouling angle (φ_f) with oil properties (see Table 1) for downflow with $v_{so}=0.15$ m/s and $v_{sw}=0.3$ m/s. It can be observed from this figure that the pressure gradient increases with an increase of oil density and fluid consistency coefficient (K), and with a decrease of flow behavior index (n), since the viscosity of the non-Newtonian oil decreases (this results agree with the data of Das et al. [45]). Similar behavior is also valid for the fouling angle. The increasing magnitude of the pressure gradient and the fouling angle depends on the range of K . When K is less than 0.01, the increasing magnitude is not significant.

Fig. 10 shows the variation of wall shear stress with oil properties for downflow with $v_{so}=0.15$ m/s and $v_{sw}=0.3$ m/s. In addition, it reveals that the wall shear stress increases with an increase of oil density and fluid consistency coefficient (K), and with a decrease of flow behavior index (n). Comparison between Fig. 9 and Fig. 10 shows that the variation of the wall shear stress is similar to that of total pressure gradient and fouling angle.

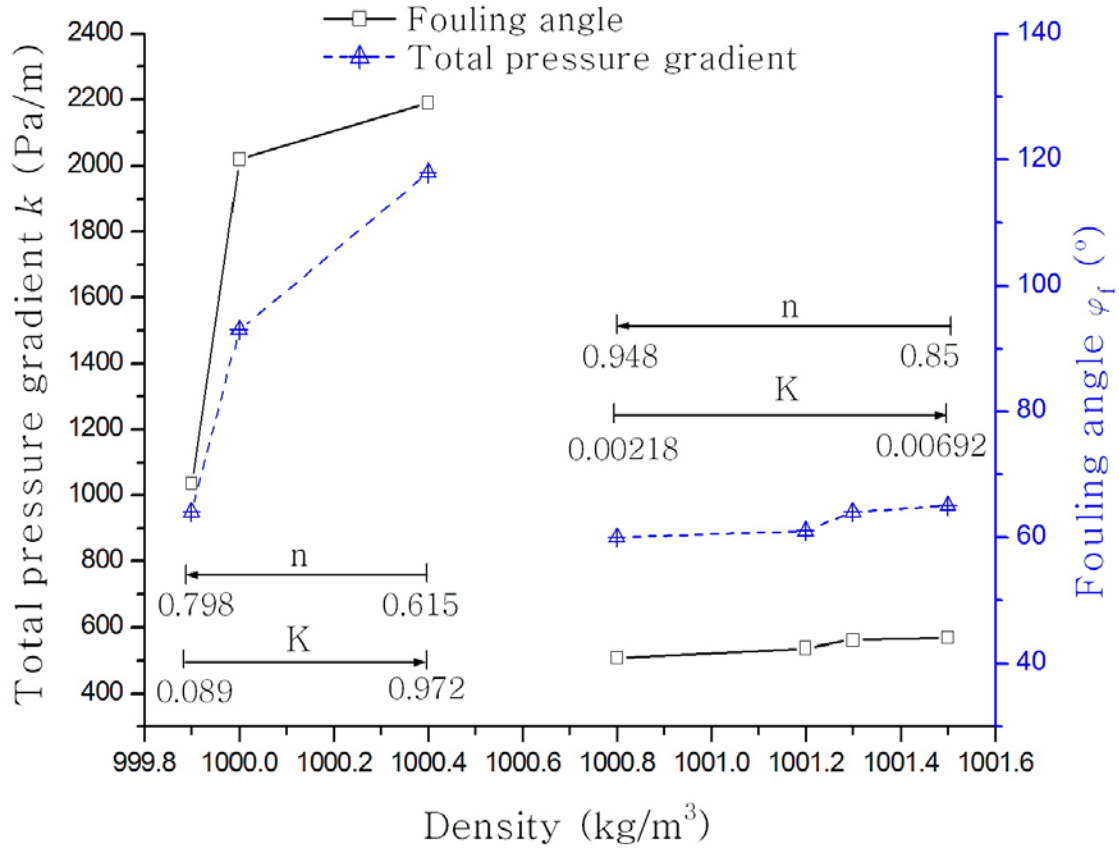


Fig. 9 Variation of total pressure gradient (k) and fouling angle (ϕ_f) with oil properties

The contours of non-Newtonian oil volume fraction at different oil properties are shown in Fig. 11. From this figure we note that the Newtonian oil can stay free from the wall throughout the whole return bend, while the non-Newtonian oil easily cling to the pipe wall. Obviously, the centrifugal force, gravity and buoyant force influence the core annular flow development. The centrifugal force tries to keep water at the outer portion of the bend curvature while non-Newtonian oil also moves toward the wall owing to buoyancy. If the buoyancy is dominating, then the oil core adheres to the outer portion of bend curvature and fouling initiates. The non-Newtonian oils of CMC1 to CMC3 have high fluid consistency coefficient (K). As K increases, the flow state in the return bend is more similar to the core annular flow. As the non-Newtonian oils of CMC4 to CMC7 have low K , the oil would stick to the outer wall of the bend at the downstream part of the pipe, because the oil with low viscosity and high density, can effortlessly break

the water film under the condition of gravity and centrifugal force. Thus, the very different behavior CMC 1-3 compared to CMC 4-7 is explained by the combination of density and fluid consistency coefficient.

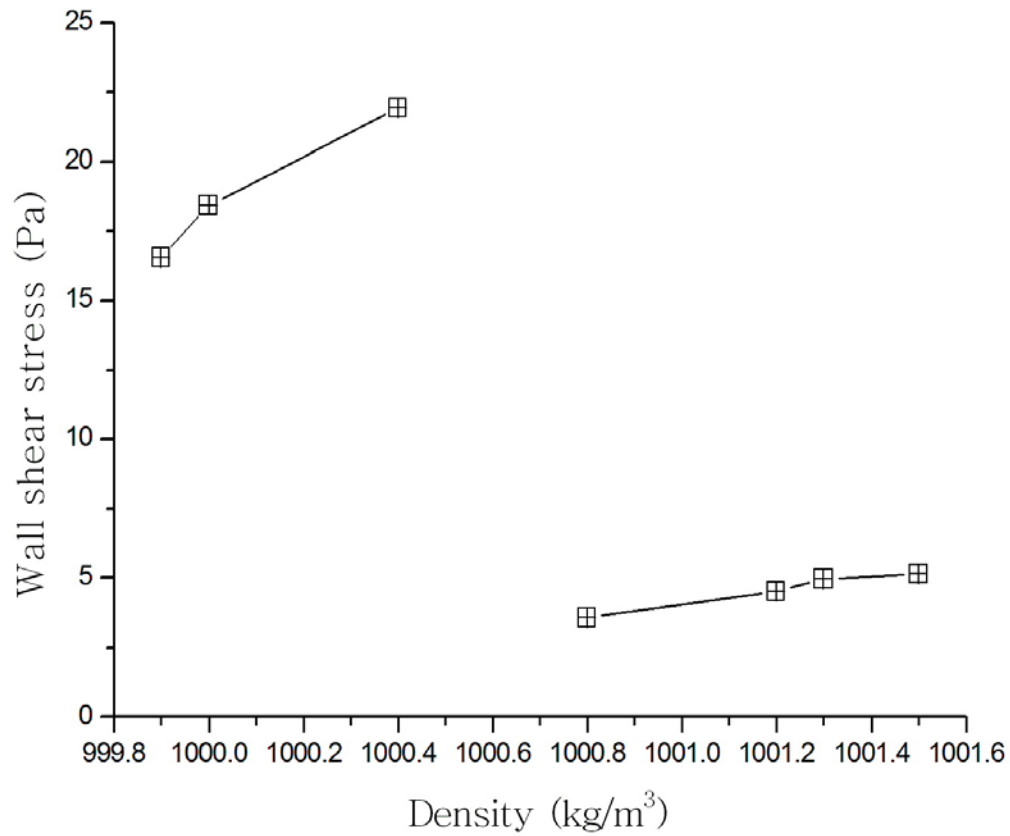


Fig. 10 Variation of wall shear stress with oil properties

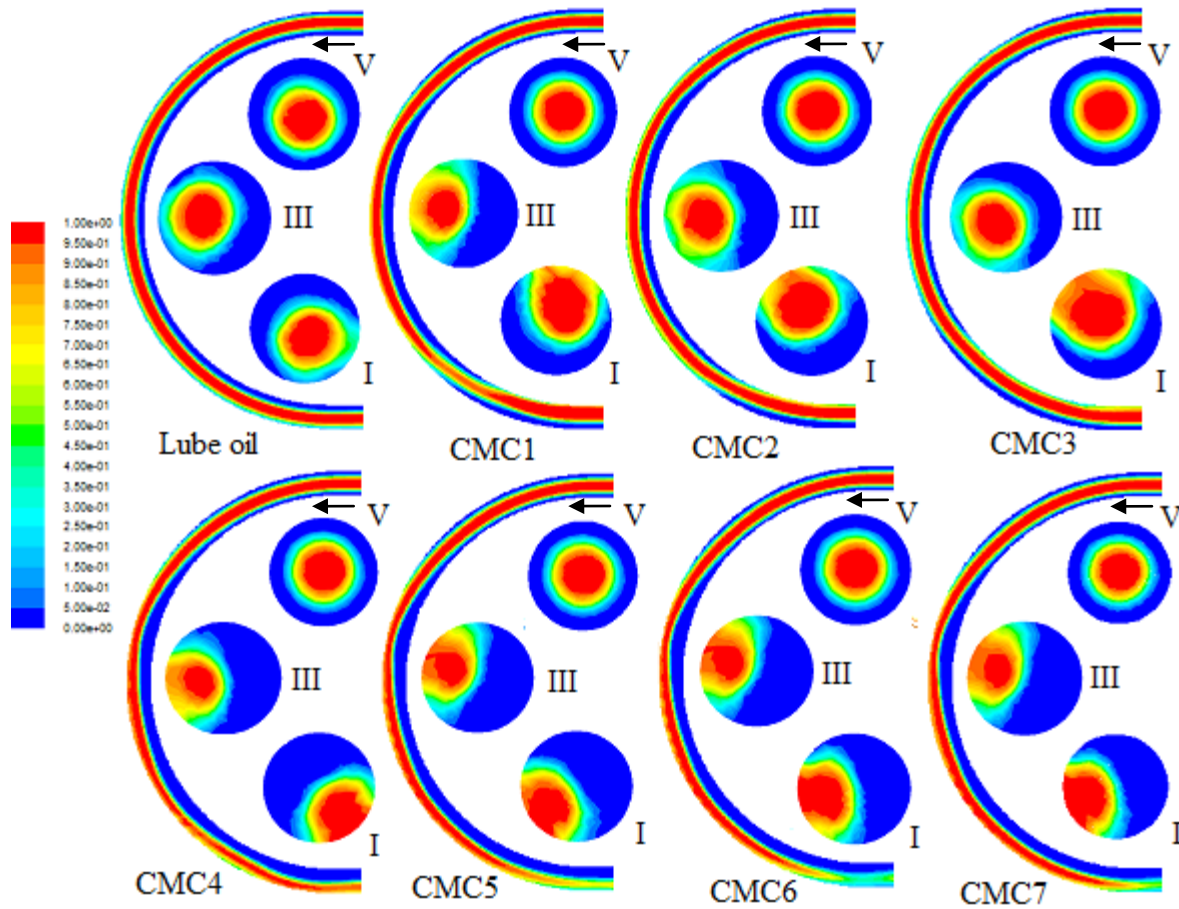


Fig. 11 Contour of the oil volume fraction for different non-Newtonian oil properties.

In order to understand the difference between non-Newtonian oil-water flow and Newtonian oil-water flow inside of the return bend, the total pressure drop and velocity distributions are shown in Fig. 12. Fig. 12a depicts the total pressure drop between cross-section I and V during core annular flow with two types of oil namely lube oil (Newtonian) and CMC 1 (non-Newtonian). It can be easily noticed that the total pressure drop has opposite distribution for the two types of oil. Fig. 12b presents the velocity profiles at the corresponding cross-sections. For Newtonian oil-water core annular flow, the velocity magnitude varies relatively little in different cross-sections. However, for non-Newtonian oil-water core annular flow, the velocity magnitude changes sharply.

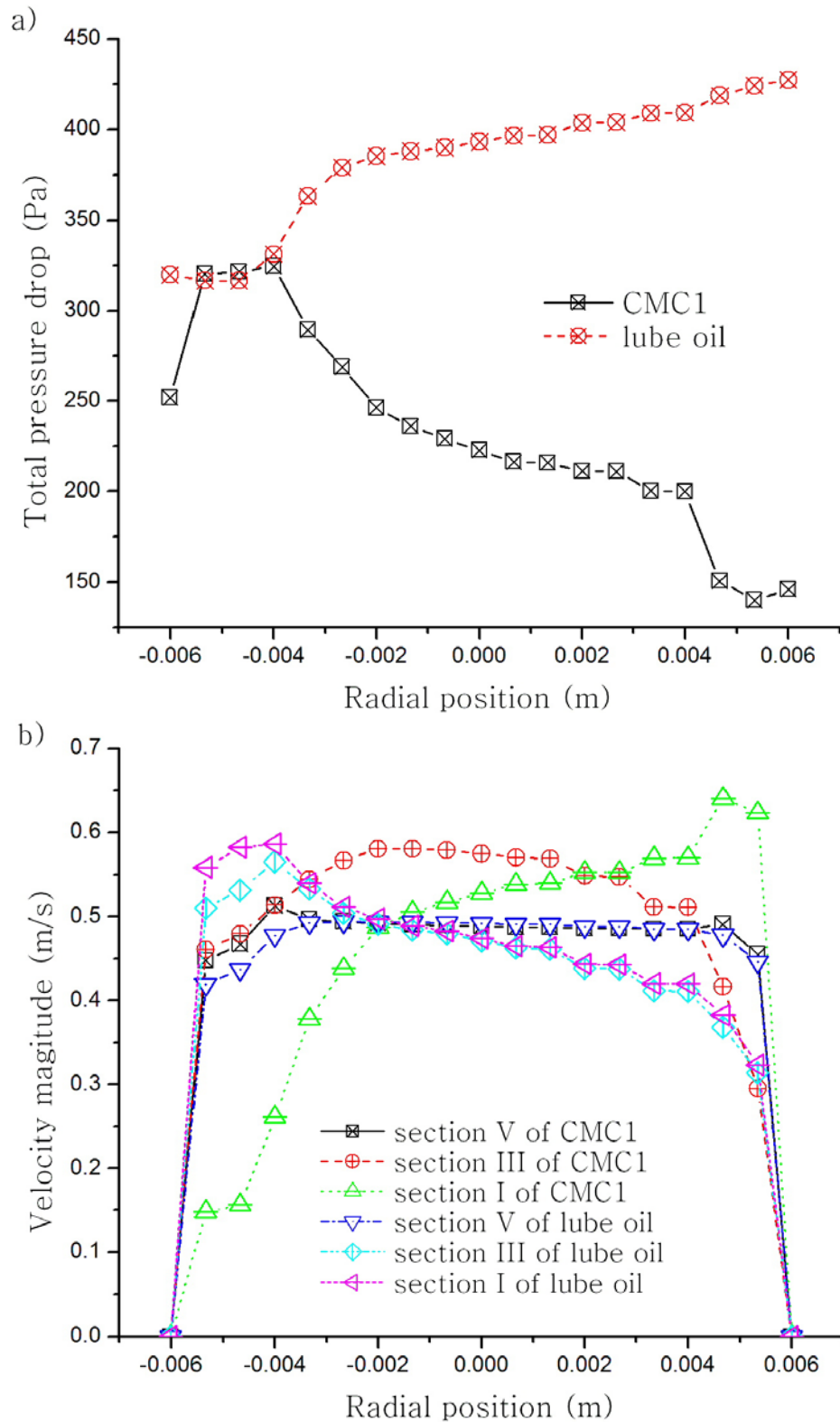


Fig. 12 Comparison of non-Newtonian oil and Newtonian oil. a) comparison of total pressure drop between positions I and V; b) comparison of velocity magnitude in different cross-sections.

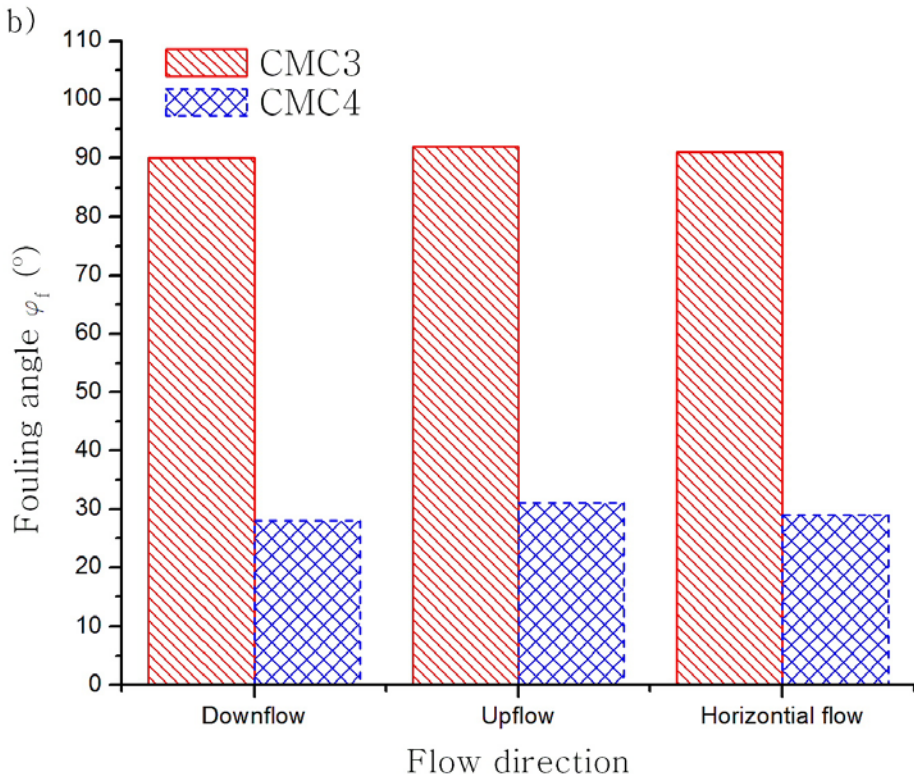
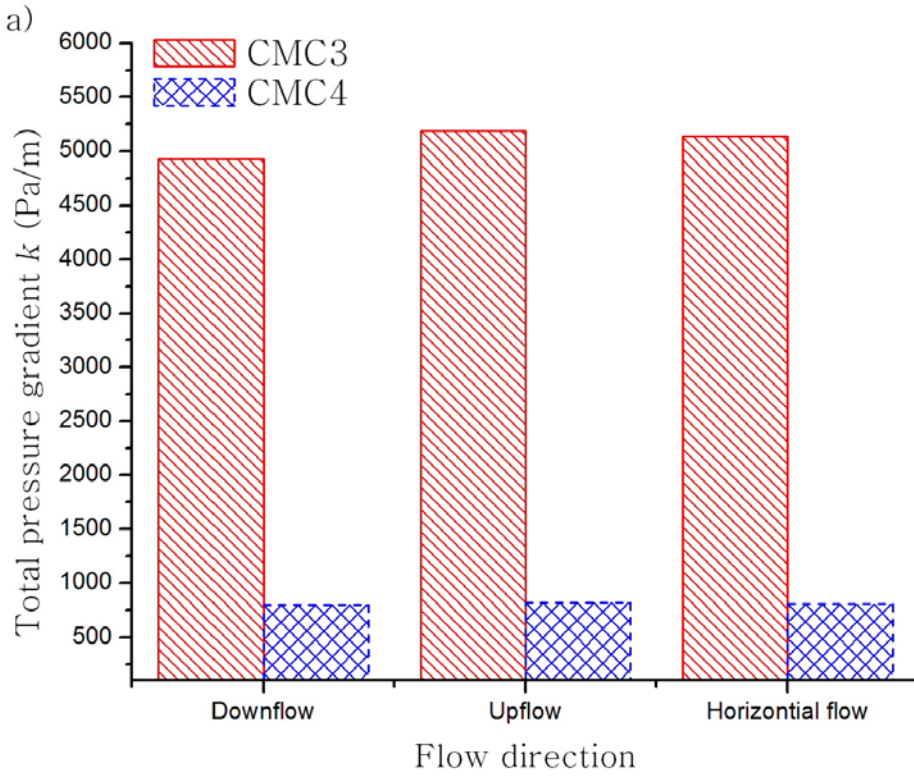


Fig. 13 Variation of total pressure gradient (k) and fouling angle (ϕ_f) with flow direction. a) total pressure gradient; b) fouling angle.

4.4 The effect of flow direction on the flow field

Attempts have next been conducted to investigate the effect of flow direction on flow field. The up, down and horizontal core annular flow (the oil is CMC 1) across return bend at $v_{so}=0.15$ m/s and $v_{sw}=0.3$ m/s are simulated. Fig. 13 shows the flow direction influence on the total pressure gradient and fouling angle. One may note that the point of initiation of fouling at the bend and the pressure gradient are not completely identical for the three flow orientations, although their values are very similar. Hence, it can be said that the flow direction has a negligible impact on the total pressure gradient and fouling angle. The only difference between the flows in the bends with three different directions is gravity. However, due to the small pipe size, the effect of pipe orientation is not great.

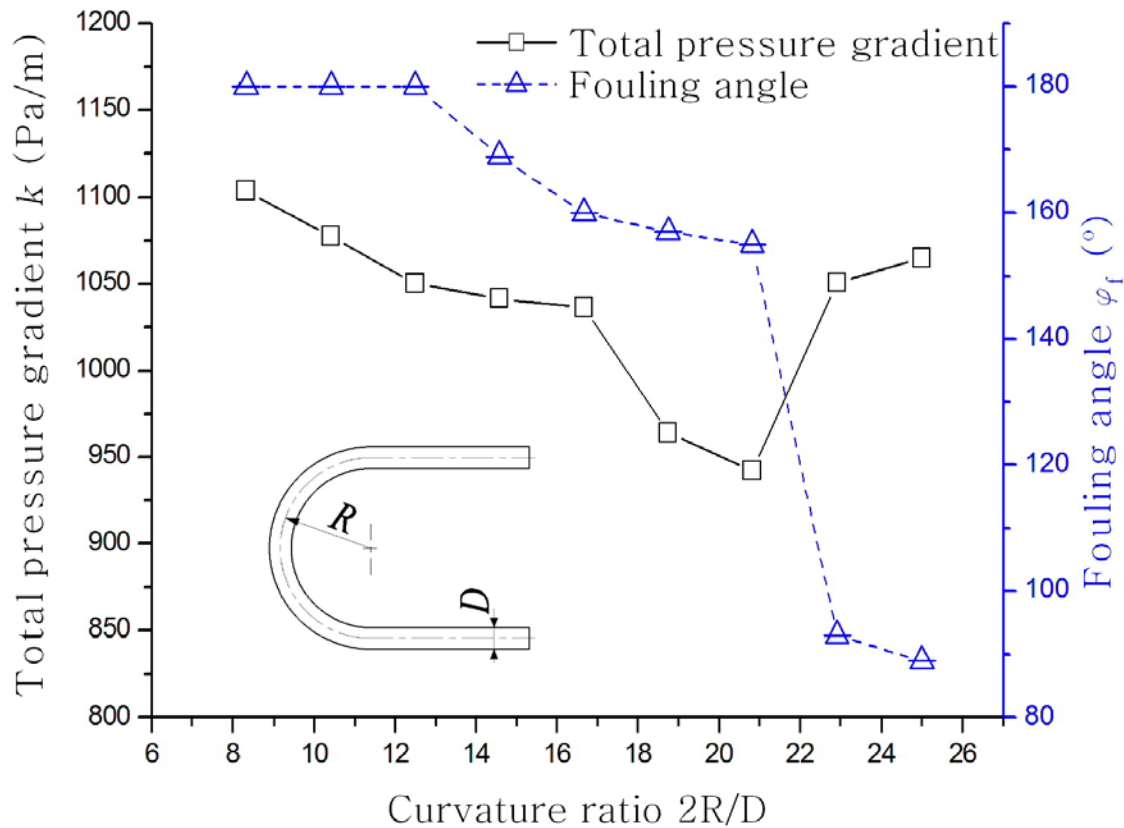


Fig. 14 Variation of total pressure gradient (k) and fouling angle (φ_f) with curvature ratio

4.5 The effect of bend parameters on the flow field

Subsequently, attempts were made to understand the influence of bend parameters on the flow field. For this study, the oil is CMC 1 and the curvature ratio is varied from 8.33 to 25. Fig. 14 represents the variation of total pressure gradient and fouling angle with bend curvature ratio ($2R/D$) for constant oil and water superficial velocity ($v_{so}=0.15$ m/s and $v_{sw}=0.3$ m/s). For mild curvature ratios, the fouling angle and total pressure gradient decrease with increasing curvature ratio. However, when $2R/D > 20$, the total pressure gradient increases sharply, while at the same time, the fouling angle decreases. The fouling angle decreases for large curvature ratio ($2R/D > 20$) due to the flow's longer exposure to the bending geometry. Consequently, the adherence of oil to the wall results in blockage which increases the pressure losses. Considering both the total pressure gradient and fouling angle, a curvature ratio of less than approximately 20 is preferable for non-Newtonian oil and water core annular flow through the return bend.

To investigate the effect of inlet diameter ratio ($D1/D$) on total pressure gradient and fouling angle, the diameter ratio is varied from 0.583 to 0.833. The variation of total pressure gradient and fouling angle with inlet diameter ratio is depicted in Fig. 15. There is a gradual increase in the total pressure gradient with the inlet diameter ratio, and after $D1/D=0.71$ the increase is dramatic. Because the inlet diameter ratio increases, the volume fraction of non-Newtonian oil also increases, which leads to an increased mixture viscosity, which in turn finally induces the pressure gradient increase. For the fouling angle, it increases until it attains a maximum at $D1/D=0.71$, after which it instead decreases with further increase of the inlet diameter ratio. The reason is that as the inlet diameter ratio increases in case of $D1/D > 0.71$, the thickness of water film decreases dramatically, and is hence easily broken by the non-Newtonian oil, which leads to the fouling to the wall.

Thus, considering both the total pressure gradient and the fouling angle for given operating conditions, an inlet diameter ratio in the range of 0.67 to 0.75 is suitable to keep the oil-water core annular flow in a return bend.

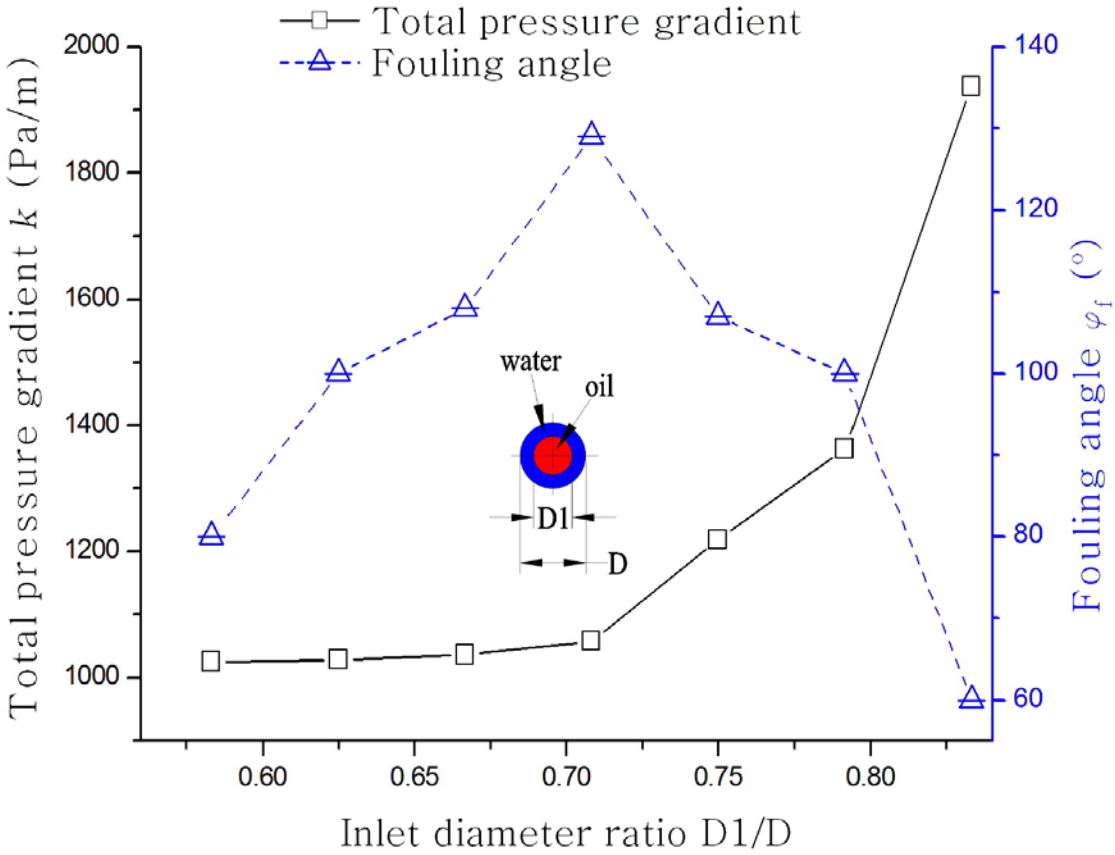


Fig. 15 Variation of total pressure gradient (k) and fouling angle (φ_f) with inlet diameter ratio

5. Conclusions

The present study aims at analyzing laminar core annular flow of non-Newtonian oil and water across return bends. For this, a three dimensional model has been developed using the CFD software FLUENT. The verification of the numerical procedure was performed by calculating the phase distribution contours of Newtonian oil and water simulation which agrees well with the empirical values [36]. From the subsequent study of non-Newtonian oil and water, the following conclusions can be made:

- (1) The VOF and CSF models can predict that the evolution of annular flow, including pressure, velocity, and wall shear stress distributions.

(2) The non-Newtonian oil properties do influence the non-Newtonian oil water core annular flow through return bends. The pressure gradient, fouling angle and wall shear stress increase with larger oil density and fluid consistency coefficient (K), or a smaller flow behavior index (n).

(3) The flow direction through the return bend has no significant effect on the total pressure gradient and fouling angle due to the small pipe diameters considered in this investigation.

(4) The geometry parameters can influence the total pressure gradient and the fouling angle as the oil-water flow through the return bend. As the curvature ratio or inlet diameter ratio are above a certain value, the total pressure gradient increases and the fouling angle decreases dramatically. For this reason, the curvature ratio should be between 16 and 20, the inlet diameter ratio in range of 0.67-0.75, for the oil-water two-phase to experience a more stable core annular flow through the return bend.

Acknowledgement

The authors gratefully acknowledge research support from the Agency for Science, Technology and Research (A*STAR) and Engineering Research Grant, SERC Grant No: 1021640147.

Conflict of interest statement

On behalf of all authors, the corresponding author states that there is no conflict of interest.

References

1. Clark AF, Shapiro A (1949) Method of pumping viscous petroleum. U.S. Patent No. 2, 533, 878
2. Oliemans RVA, Ooms G, Wu HL, Duijvestijn A (1987) Core annular oil/water flow: the turbulent-lubricating-film model and measurements in a 5 cm pipe loop. *Int. J. Multiphase Flow* 13: 23- 31
3. Bai R, Chen K, Joseph DD (1992) Lubricated pipelining: stability of core-annular flow: part 5. Experiments and comparison with theory. *J. Fluid Mechanics* 19:97-132
4. Arney MS, Bai R, Guevara E, Joseph DD, Liu K (1993) Friction factor and holdup studies for lubricated pipeline-I: Experiments and correlations. *Int. J. Multiphase Flow* 19: 1061-1076

5. Rodriguez OMH, Oliemans RVA (2006) Experimental study on oil-water flow in horizontal and slightly inclined pipes. *Int. J. Multiphase Flow* 32:323-343
6. Sotgia G, Tartarini P, Stalio E (2008) Experimental analysis of flow regimes and pressure drop reduction in oil-water mixtures. *Int. J. Multiphase Flow* 34:1161-1174
7. Strazza D, Grassi B, Demori M, Ferrari V, Poesio P (2011) Core-annular flow in horizontal and slightly inclined pipes: Existence, pressure drops, and hold-up. *Chem. Eng. Sci.* 2853-2863
8. Strazza D, Poesio P (2012) Experimental study on the restart of core-annular flow. *Chem. Eng. Res. Des.* 90:1711-1718
9. Ooms G, Seoal A, Vanderwees AJ, Meerhoff R, Oliemans RVA (1984) A theoretical model for core-annular flow of a very viscous oil core and a water annulus through a horizontal pipe. *Int. J. Multiphase Flow* 10: 41-60
10. Brauner N (1991) Two-phase liquid liquid annular flow. *Int. J. Multiphase Flow* 17:59-76
11. Prada JWV, Bannwart AC (2001) Modeling of vertical core-annular flows and application to heavy oil production. *J. Energ. Resour. Technol.* 123:194-199
12. Ooms G, Vuik C, Poesio P (2007) Core-annular flow through a horizontal pipe: Hydrodynamic counterbalancing of buoyancy force on core. *Phys. Fluid* 19:092103
13. Rodriguez OMH, Bannwart AC, Carvalho CHM (2009) Pressure loss in core-annular flow: Modeling, experimental investigation and full-scale experiments. *J. Petro. Sci. Eng.* 65:67-75
14. Ooms G, Pourquie MJB., Beerens JC (2013) On the levitation force in horizontal core-annular flow with a large viscosity ratio and small density ratio. *Phys. Fluids* 25:032102
15. Bai T, Kelkar K, Joseph DD (1996) Direct simulation of interfacial waves in a high viscosity ratio and axisymmetric core annular flow. *J. Fluid Mechanics* 327:1-34
16. Li J, Renardy Y (1999) Direct simulation of unsteady axisymmetric core-annular flow with high viscosity ratio. *J. Fluid Mech.* 391:123-149
17. Ko T, Choi HG, Bai R, Joseph DD (2002) Finite element method simulation of turbulent wavy core-annular flows using a k-w turbulence model method. *Int. J. Multiphase Flow* 28:1205-1222
18. Ooms G, Pourquie MJB., Poesio P (2012) Numerical study of eccentric core-annular flow. *Int. J. Multiphase Flow* 42:74-79
19. Dong XH, Liu HQ, Wang Q, Pang ZX, Wang CJ (2013) Non-Newtonian flow characterization of heavy crude oil in porous media. *J. Petrol. Explor. Prod. Technol.* 3:43-53
20. Edwards MF, Jadallah MSM, Smith R (1985) Head losses in pipe fittings at low Reynolds numbers. *Chem. Eng. Res. Dev.* 63:43-50

21. Banerjee TK, Das M, Das SK (1994) Non-Newtonian liquid flow through globe and gate valves. *Can. J. Chem. Engg.* 72:207-211
22. Turian RM, Ma TW, Hsu FLG, Sung MDJ, Plackmann GW (1998) Flow of concentrated non-Newtonian slurries: 2. Friction losses in bends, fittings, valves and venture meters. *J. Multiphase Flow* 24: 243-269
23. Bandyopadhyay TK, Das SK (2007) Non-Newtonian pseudoplastic liquid flow through small diameter piping components. *J. Petrol. Sc. & Engg.* 55:156-166
24. Xu JY, (2010) Investigation on average void fraction for air/non-Newtonian power-law fluids two-phase flow in downward inclined pipes. *Exp. Therm. Fluid Sci.* 34:1484-1487
25. Cruz DA, Coelho PM, Alves MA (2012) A simplified method for calculating heat transfer coefficients and friction factors in laminar pipe flow of non-Newtonian fluids. *J. Heat Transfer* 134: 091703
26. Srivastava RPS (1977) Liquid film thickness in annular flow. *Chem. Eng. Sci.* 28: 819-824
27. Lennon ON, Peter DMS (2010) Interfacial instability of turbulent two-phase stratified flow: Pressure-driven flow and non-Newtonian layers. *J. Non-Newtonian Fluid Mech.* 165:489-508
28. Li HW, Wong TN, Skote M, Duan F (2013) A simple model for predicting the pressure drop and film thickness of non-Newtonian annular flows in horizontal pipes. *Chem. Eng. Sci.* 102:121-128
29. Usui K, Aoki S, Inoue A (1980) Flow behavior and pressure drop of two-phase flow through C-shaped bend in vertical plane, (I) upward flow. *J. Nuclear Sci. Technol.* 17:875-887
30. Chen IY, Yang YW, Wang CC (2002) Influence of horizontal return bend on the two-phase flow pattern in 6.9 mm diameter tubes. *Canadian Journal of Chemical Engineering*, 82:478-484
31. Wang CC, Chen IY, Yang YW, Hu R (2004) Influence of horizontal return bend on the two-phase flow pattern in small diameter tubes. *Exp. Therm. Fluid Sci.* 28:145-152
32. Kerpel KD, Ameel B, Huisseune H, T'Joene C, Caniere H, Paepe MD (2012) Two-phase flow behavior and pressure drop of R134a in a smooth hairpin. *Int. J. Heat Mass Transfer* 55:1179-1188
33. Padilla M, Revellin R, Wallet J, Bonjour J (2013) Flow regime visualization and pressure drops of HFO-1234yf, R-134a and R-410A during downward two-phase flow in vertical return bends. *Int. J. Heat Fluid Flow* 40:116-134
34. Meng M, Yang Z, Duan YY, Chen Y (2013) Boiling flow of R141b in vertical and inclined serpentine tubes. *Int. J. Heat Mass Transfer* 57:312-320
35. Sharma M, Ravi P, Ghosh S, Das G, Das PK (2011) Studies on low viscous oil-water flow through return bends. *Exp. Therm. Fluid Sci.* 35:455-469
36. Sharma, M., Ravi. P., Ghosh S., Das, G., Das P.K., 2011b. Hydrodynamics of lube oil-water flow through 180° return bends. *Chem. Eng. Sci.*, 66: 4468-4476

37. Ghosh, S., Das, G., and Das, P.K., 2011. Simulation of core annular in return bends – a comprehensive CFD study. *Chem. Eng. Res. Design*, 89: 2244-2253
38. Jiang F, Long Y, Wang YJ, Liu ZZ, Chen CG (2016) Numerical simulation of Non-Newtonian core annular flow through rectangle return bends. *J. Appl. Fluid Mech.* 9: 431-441
39. Skote M (2014) Scaling of the velocity profile in strongly drag reduced turbulent flows over an oscillating wall. *Int. J. Heat Fluid Flow* 50:352-358
40. Brackbill JU, Kothe DB, Zemach C (1992) A continuum method for modeling surface tension. *J. Comput. Phys.* 100: 335-354
41. Jiang F, Wang YJ, Ou JJ, Xiao ZM (2014) Numerical simulation on oil-water annular flow through the Π bend. *Ind. Eng. Chem. Res.*,53:8235-8244
42. Shosh S, Das G, Das PK (2011) Pressure drop analysis for liquid-liquid downflow through vertical pipe. *J. of Fluids Eng.* 133:011202
43. Xu JY, Wu YX (2009) A simple model for predicting the void fraction of gas/non-Newtonian fluid intermittent flows in upward inclined pipes. *Chem. Eng. Comm.* 196:746-753
44. Maiumder SK, Kundu G, Mukheriee D (2007) Pressure drop and bubble-liquid interfacial shear stress in a modified gas non-Newtonian liquid downflow bubble column. *Chem. Eng. Sci.* 62:2482-2490
45. Das SK, Biswas MN, Mitra AK (1991) Non-newtonian liquid flow in bends. *Chem. Eng. J.* 45: 165-171